A STOCHASTIC DYNAMICS MODEL OF BEAM OBSTACLE TRAVERSAL IN TWO DIMENSIONS

by

Bokun Zheng

A thesis submitted to The Johns Hopkins University in conformity with the requirements for the degree of Master of Science.

Baltimore, Maryland

May, 2021

Abstract

Animals are excellent locomotors at traversing obstacles in complex terrain. Recent studies in our lab discovered that the potential energy landscape helps understand how animals' and robots' transition between locomotor modes. In that study, the energy landscape model was quasi-static and did not capture stochastic dynamics common in locomotion. In addition, obstacles were uniform; however, in the nature world, obstacles are rarely symmetric. Here, I take the next step in establishing a stochastic dynamics simulation on a simplistic 2-D model system, a self-propelled circular body interacting with two adjacent horizontal elastic beam obstacles on a horizontal flat ground. Body-beam interaction was determined by calculating collisional dynamics between rigid bodies and solving the interaction force by constraint conditions. On the landscape, the resistance of the two beam obstacles resulted in a potential energy barrier on each side. I found that increasing random force and self-propulsive force increased the body's probability to overcome the barriers to traverse. By setting different stiffness, I can create a landscape with asymmetric barriers, and the body had a higher probability to escape by moving along trajectories that over-

ABSTRACT

came the lower barrier. This simple model revealed that potential energy landscapes

can be a useful tool to help understand the beam obstacle traversal process.

Primary Reader and Advisor: Chen Li

Secondary Reader: Noah Cowan

Acknowledgments

I would like to express my deepest gratitude for Prof. Chen Li providing me this opportunity working in his group in the past one and half years. He introduces and guides me into the scientific research. His passion and dedication to science has always motivated me to improve myself.

I would also like to thank Mr. Qihan Xuan, for the endless help, support, and knowledge he has given me during my Master. Without a doubt, he has been one of the best teachers I have had at Johns Hopkins.

Finally, I would like to thank people in the Terradynamics lab for the supporting atmosphere. Mr. Ratan Othayoth did prior work in this subject and provided great guidelines for following work. Mr. Yaqing Wang, Mr. Eugene Lin, and Mr. Qiyuan Fu also gave me helpful advice and inspiring discussion.

Special thanks to Prof. Noah Cowan to be the reader for this essay. His comments are very valuable for perfecting this thesis.

Dedication

I would like to dedicate this thesis to my parents, Zhong Zheng and Xueying Gao, who provide me this opportunity to study abroad, and my girlfriend, Lin Miao, for all her love and support.

Contents

CONTENTS

List of Tables

List of Figures

Chapter 1

Introduction

Animals are excellent at terrestrial locomotion [1]. Unlike mobile robots that focus on the navigation to avoid obstacles [2] [3] [4], animals are good at using their bodies and appendages to make physical interaction with the environment [5] [6]. They are also good at moving through complex terrain with obstacles comparable to the body size [7]. Understanding those biological movements can give us inspiration in designing robots with better locomotion ability [8].

The example animal studied by our lab is the Discoid cockroach (*Blaberus discoidalis*) [9], a tropical animal living in the rainforest floor filled with vegetation. Previous studies show the cockroach can take advantage of its streamlined body shape [5] to make transitions between different locomotor modes when traversing the grass-like beam obstacles.

For vertical elastic beam obstacles, the cockroach takes multiple pathways to

traverse. The recent study from our lab [10] focused on two maneuvers to traverse: pitch and roll mode, which is described in Euler angles of the body orientation (Fig. 1.1(a)). In the pitch mode, the animal pushes against the beam while pitching up. In the roll mode, the animal rolls its body into the gap between beams. A potential energy landscape approach (Fig. 1.1(b)) was used to help understand the probabilistic transitions.

A potential energy landscape can be analogous to a free energy landscape in the field of protein folding [11]. During the protein folding, the system statistically transitions via different pathways where ultimately the energy state goes from high to low. Thermal fluctuation can help cross energy barriers. Surprisingly, in the locomotor-terrain interaction systems which are self-propelled and far-from-equilibrium, a potential energy landscape is a good approach to analyze stochastic multi-pathway transitions. For example, in the previous study of the cockroach's pitch-to-roll transition, the body movement was attracted by the energy basin (local minimum, Fig. 1.1(b)), and extra kinetic energy fluctuation could help the system escape across relatively lower energy barrier [10].
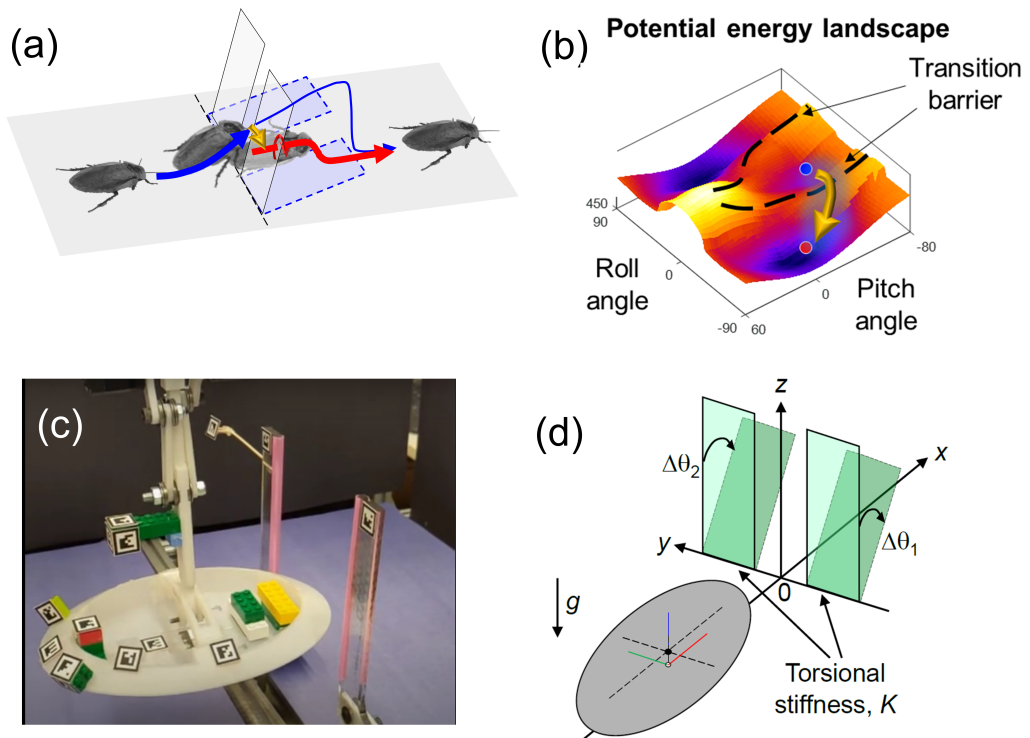
Figure 1.1: An potential energy landscape approach to locomotor transition doing beam obstacle traversal in 3D. (a) The cockroach traverses beam obstacles via different pathways. The blue curve is the pitch mode while the red curve is the roll mode. (b) Potential energy landscape with body orientations. (c) A 3D robot to study the transition in crossing beam obstacles. (d) modeling of the 3D robot in (c). Both beams have the same stiffness.
Note: Adapted from "An energy landscape approach to locomotor transitions in complex 3D terrain," by R Othayoth, G Thoms and C Li, 2020, *Proceedings of the National Academy of Sciences, 117(26)*, p.14987-14995. Copyright 2020 by National Academy of Sciences.

Our lab has also created an 3D robophysical model (Fig. 1.1(c)(d)) to emulate the cockroach's behaviors. The robot was free to rotate in body pitch or roll, with a constant forward speed to interact with two vertical elastic beams. Then, the body could enter pitch-to-roll transitions as observed on the animal. This robot was useful for studying the transitions in body orientation, but dynamics was not modeled.

CHAPTER 1. INTRODUCTION

Adding dynamic interaction for a 3D body is complex due to its high degrees of freedom. Here I take the next step to extend this self-propelled system into a fully dynamic model with stochasticity. The system is simplified to a horizontal 2D model with reduced degrees of freedom and horizontal elastic beam obstacles, and further I use this 2D model to test if the potential landscape approach can help understand obstacle traversal.

Another purpose of this study is to involve random force and test its impact on the beam obstacle traversal problems. Randomness widely exists in animal locomotion, either from the natural environment [12] or the biological system itself [13]. Although random noise is commonly designed to be avoided or reduced in the artificial system, it can play a positive role in the biological system. Randomness is beneficial in animals' behaviors such as flying [14], walking [15], preying [16], sensing [17], self-righting [18]. Random force is a common form of randomness that can be observed from the oscillations of the animal's appendages, such as tails, legs, and wings [19] [20] [21]. On the potential energy landscape, kinetic energy fluctuation by random oscillations can increase the probability of escaping energy barriers.

Asymmetry is another factor to be tested in this study. In the previous beam-obstacle traversal experiment, the two vertical beams were the same. However, such symmetry is rarely found in the natural environment, and asymmetry plays an important role in animal locomotion [22] [23]. In this study, the asymmetry is created by a pair of beams with same geometry but different torsional stiffness. When the

CHAPTER 1. INTRODUCTION

body pushes the beams forward, the asymmetry in stiffness can lead to asymmetric reactive forces and potential energy barriers.

My study develops a 2D stochastic dynamics model to study horizontal beams traversal process. Chapter 2 introduces the model setup (Section 2.1) with two dynamics methods: the collision method (Section 2.2) and the constraint method (Section 2.3). The potential energy landscape is defined in Section 2.5. Chapter 3 discusses the results of simulation designed to test two hypotheses: (1) The body has a higher probability of traversal over symmetric beam obstacles under larger self-propulsive force and random force (Section 3.1). (2) The asymmetry on the landscape will lead to an increased traversal probability on the lower barrier side (Section 3.2). Further, the single pair of beam obstacles are extended to a larger multi-obstacle field (Section 2.6) and statistical tests are conducted over it (Section 3.3). I also made the attempt to realize the model with a real robot (Section 2.9). Chapter 4 summarizes the work (Section 4.1) and discusses the contributions (Section 4.2), limitations, and future work (Section 4.3).

Chapter 2

Model development

2.1 Model description

A simulation model is developed in MATLAB. The model (Fig. 2.1(b)(c)) includes three rigid bodies: A pair of elastic beam obstacles and one locomotor body. Each horizontal beam can rotate about a revolute joint. The body can move freely on a 2D horizontal plane without friction between ground or beams. Note that only the 2D structure (Fig. 2.1(c)) is realized in the simulation. The 3D schematic diagram (Fig. 2.1(b)) is just for better understanding the layout.

The body model is inspired by the Lateral Leg Spring template [24] from the cockroach (Fig. 2.1(a)). When the cockroach moves forward, it is a self-propelled object. The spring-like legs on lateral side can provide extra vibration in kinetic energy. My model is designed after simplification and approximations based on the
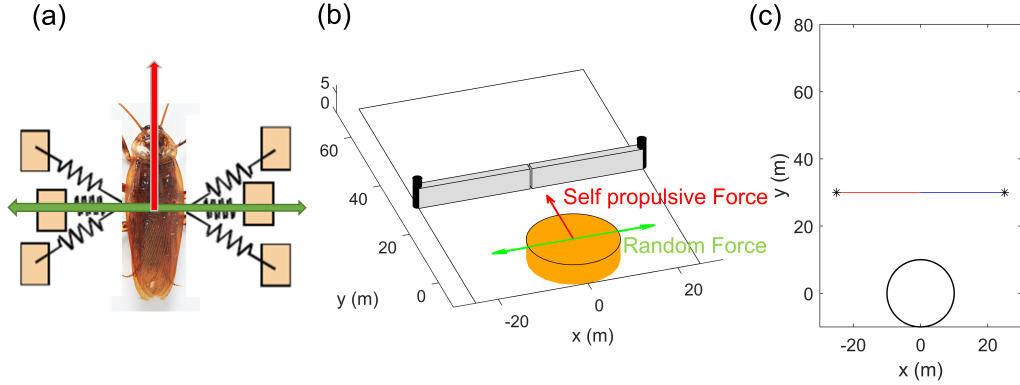
LLS model.

Figure 2.1: Cockroach inspired simulation model. (a) Lateral Leg Spring (LLS) model of the cockroach legs. (b) 3D schematic diagram of the model layout, with forward self-propulsive force and lateral random force (c) Visualization in the simulation. The circle represents the body, and the blue/red line represents the left/right beam.

In my model, the body shape is approximated to a circular disk moving on a 2D horizontal plane. There are several assumptions for the body: (1) Body mass is uniformly distributed. (2) External forces are applied at the center of mass. (3) The body surface and bottom is smooth and frictionless. (4) The body orientation is constantly pointing to the fore-after axis. No external torque is applied to the body so that the body orientation will remain unchanged. The horizontal beam has the following assumptions: (1) The beam is rigid without thickness and can only rotate about the revolute joint. (2) Mass is equally distributed. (3) The joint is torsional elastic with viscous damping.

Based on these assumptions, a constant self-propulsive force F_{prop} is defined, pointing to the y-direction. Then the lateral random force F_{rand} is parallel to the x-axis.

CHAPTER 2. MODEL DEVELOPMENT

When the beam rotates about the joint, it needs to overcome the torque consisting of elasticity which is proportional to the angle, and viscous damping which is proportional to the angular velocity. The equations of motion are:

$$\text{Body: } Ma = F_{prop} + F_{rand} + \sum F^i_{resis} \tag{2.1}$$

$$\text{Beam: } I\beta_i = -F^i_{resis} - k_i\theta_i - d_i\omega_i \tag{2.2}$$

where M is the body mass, a is the body acceleration, F_{prop} is the random force, F_{rand} is the random force, F^i_{resis} is the resistance force acting at the body from the ith beam, $i = 1$, 2 for left and right beam respectively, I is the moment of inertia at the joint, $\theta_i, \omega_i, \beta_i$ are the rotated angle, angular velocity, and angular acceleration of the ith beam, k_i is the stiffness coefficient of the ith joint, and d_i is the damping coefficient of the ith joint.

Table 2.1 shows the model parameters:

Table 2.1: Model parameters

Parameter	Value
Body mass M	1 kg
Body radius R	10 m
Beam length L	25 m
Beam mass m	0.1 kg
Beam inertia I	20.83 kg m^2

The lateral random force F_{rand} is designed to randomly change magnitude and swiching direction along the x-axis at a given frequency. The *Gaussian Random*

Number Generator in MATLAB can produce a range of random force (Fig. 2.2) by multiplying the random number *randn* with a constant amplifier magnitude *Rm*, which is used as a variable (Eqn. 2.3).

$$F_{rand} = Rm \times randn \tag{2.3}$$

where Rm is the random number magnitude, and $Randn$ is a random number that conforms the standard normal distribution.
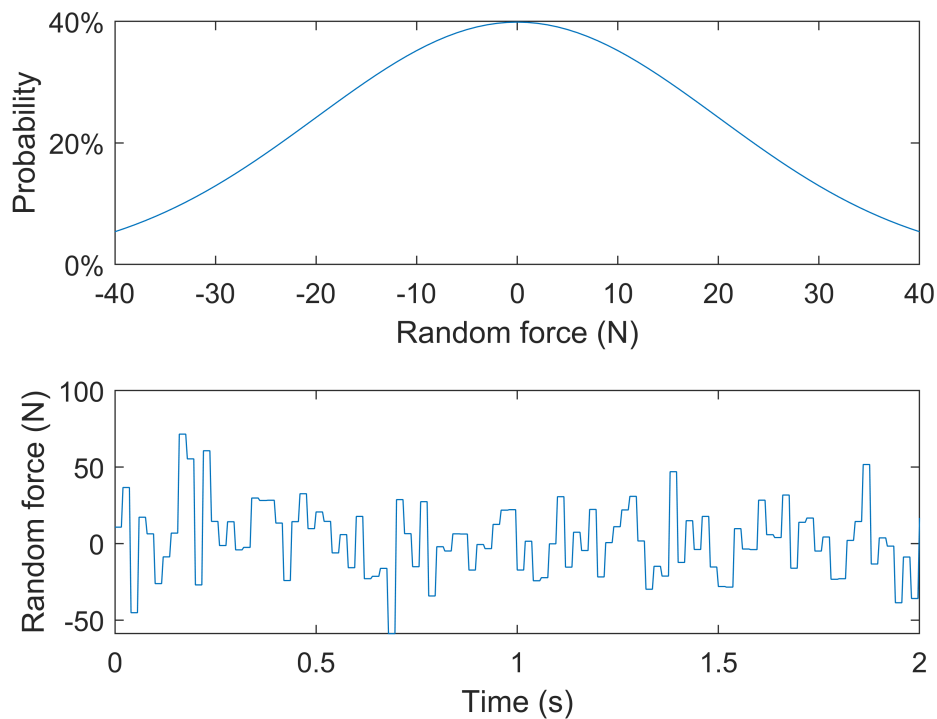
Figure 2.2: Random force example at $Rm = 20N$. Upper: probability distribution of the random force. Lower: An example of random force changing at 50 Hz.

The dynamics is the key part of the simulation. The discrete numerical integration

is used to calculate the evolution of velocities and positions over time. The time step is 0.004s to balance numerical accuracy and computational efficiency. At each time step, the dynamics of the body and beams are integrated from the prior time step.

The interaction between the body and beams need to be determined in order to implement the multi-body dynamics. Here I take two approaches: the collision method and the constraint method. Different approaches have different applicable conditions and further will be integrated together in a single simulation. This will be introduced in detail in Section 2.4.

2.2 Collision method

The collision method is one approach to determine the interaction between body and beams. The basic idea is to have the body and beam repeatedly collide and depart. Because the body is self-propelled forward and beams are resisted by the torque, the opposite moving trends can ensure the numerical convergence after continual collisions.

2.2.1 Contact and collision detection

In multi-body simulation, collision detection is an important issue [25] [26]. Here, the detection procedure contains two parts: contact detection and collision detection.

Contact detection finds the closest point on the beam to the body and measures

the shortest distance from this closest point to the center of the body. If the distance is less than body radius, the body will intersect with the beam. There are two different types of contact. In the tangent contact case (Fig. 2.3), the beam is tangent to the body. In the point contact case (Fig. 2.4), the beam touches the body at the end. The different geometric relationships in each case will lead to different ways to implement the following collision detection and collision processes.

Then, collision detection will check whether the velocities satisfy the collision condition. It will first use contact detection to detect the current contact case. According to different cases, it will compute the normal velocities at the contacting point. The collision happens when two conditions are satisfied: (1) The body and beam have contact. (2) There are opposite normal velocities at the contacting point.

2.2.2 Collision

The collision happens between two objects. In multi-body collisions, the order of collisions need to be decided first. In my model, this can happen when the body collides with both beams together in the same time step. The order of collisions is decided by comparing the distances of small gaps between contacting objects, which exist because of the tolerance of numerical error. In other words, the beam which is closer to the body will collide first.

During the collision process, the momentum exchanges instantaneously along the normal direction. The collision calculation is separated according to the contact cases,

in which the normal directions along the contacting interface are different.

Here the body and beam can be treated as a system with the center of rotation at the beam joint. At the instantaneous collision moment, time can be considered as infinitesimal. After multiplying with the finite beam joint torque, the angular impulse can be neglected. The impulse from the finite external forces acting on the body such as the self-propulsive force and the random force can be neglected in the same way. In addition, the external force acting from the joint to the beam is passing the beam joint as the center of rotation and does not generate the external torque. Therefore, the angular momentum of the system about the instantaneous center of rotation is conserved at collision.

2.2.2.1   Collision in the tangent contact case

In the tangent contact case (Fig. 2.3), the normal direction is perpendicular to the beam. The normal velocity of the body and the local velocity of the beam are in the same line.

To better emulate the collision in real physical model, the conservation of energy is not expected. Here the collision elasticity is controlled by the coefficient of restitution, CoR, which is the ratio of the final to initial relative velocity between two objects after they collide and it reflects how much energy is conserved. Eqn. 2.5 is the definition of CoR in my model, which can be set to range from 0 to 1, where 0 is perfectly inelastic collision, and 1 is perfectly elastic collision. Ideally, CoR should

be measured from a real physical model. Here it is set to be 0.8 to conserve a large

part of the energy at each collision so that the traversal will be possible after a series

of collision. It is also flexible to be changed as a parameter.
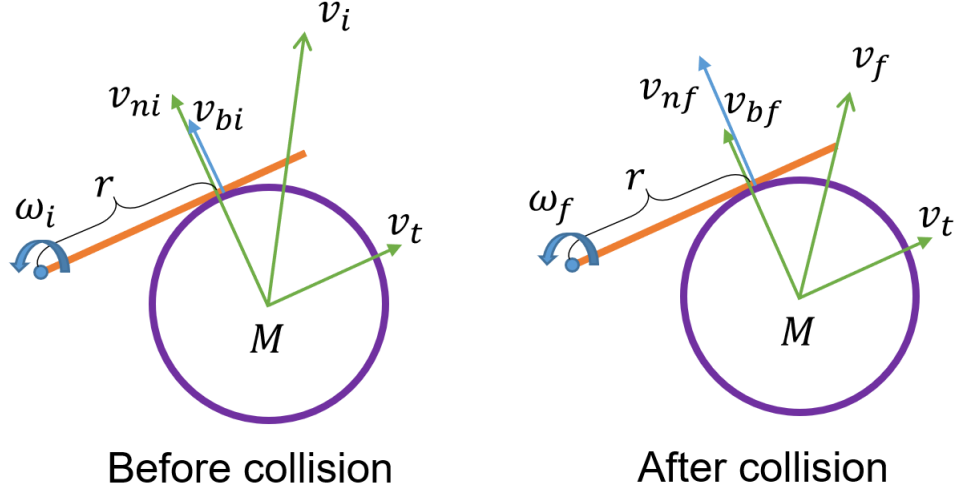
Figure 2.3: Schematic diagram of the tangent contact case before and after a collision. Here the orange line represents the left beam, the purple circle represents the body, ω_i and ω_f are the beam angular velocity before and after the collision, v_{bi} and v_{bf} are the local velocity at the contacting point on the beam before and after the collision, v_{ni} and v_{nf} are the body normal velocity before and after the collision, v_i and v_f are the body velocity before and after the collision, and v_t is the body tangent velocity that remains constant during the collision, and r is the distance from the joint to contacting point.

By using the expression of CoR (Eqn. 2.5) and the conservation of angular momentum (Eqn. 2.4), the velocities after collision, v_f and ω_f, can be solved.

$$mrv_{ni} + I\omega_i = mrv_{nf} + I\omega_f \tag{2.4}$$

$$CoR = \frac{v_{nf} - r\omega_f}{r\omega_i - v_{ni}} \tag{2.5}$$

where ω_i and ω_f are the angular velocity before and after the collision, v_{ni} and v_{nf} are the normal velocity before and after the collision, and r is the distance from the joint to contacting point.

2.2.2.2   Collision in the point contact case

In the point contact case (Fig. 2.4), the normal direction is not perpendicular to the beam. The local velocity of the beam end is not in line with the normal direction. Unlike the tangent contact case, the velocity must be expressed in vector form for calculation. So, it is more complex to formulate a CoR expression like Eqn. 2.5, though mathematically it is feasible.

Thus, for simplicity, an assumption is made that the collision in the point contact case is perfectly elastic. In addition, the relative velocity is usually low when the body arrives at such position, so that the energy loss in low-energy-exchange collisions is not significant for the whole process.

Also, similar to the assumption for conservation of angular momentum, within an infinitesimal time interval, the angular work done by the finite beam joint torque and the work done by the finite self-propulsive force and random force can be neglected instantaneously. In addition, the beam joint is fixed so the interaction force between the beam and joint cannot do work. Therefore, both the external and internal interactions in the system are instantaneously energy conserved. The system satisfies the conservation of energy at collision.
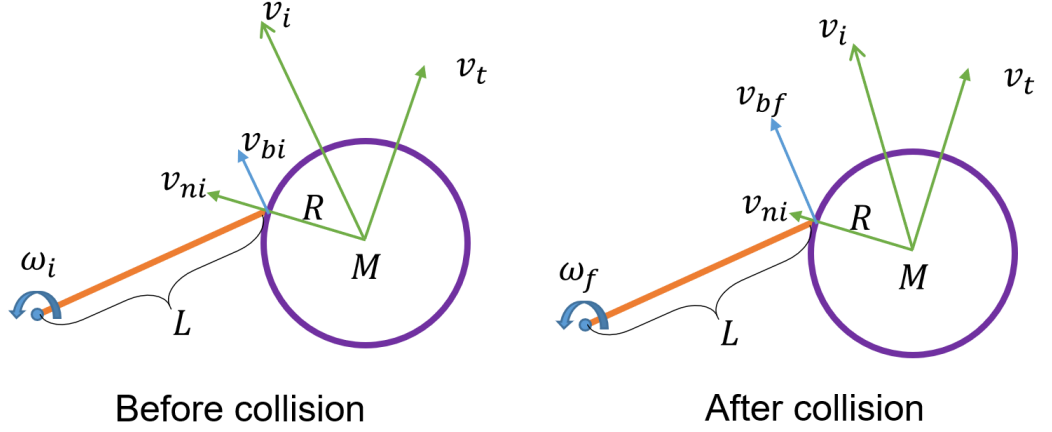
Figure 2.4: Schematic diagram of the point contact case before and after a collision. Here the orange line represents the left beam, the purple circle represents the body, L is the length of the beam.

The velocities after collision, v_f and ω_f can be solved by the conservation of angular momentum (Eqn. 2.6, 2.7, 2.8) and energy (Eqn. 2.9):

$$\Delta P = M(v_f - v_i) = F\Delta t \tag{2.6}$$

$$\Delta L_{beam} = I(\omega_f - \omega_i) = -r \times F\Delta t \tag{2.7}$$

$$\Delta L_{sys} = r \times \Delta P + \Delta L_{beam} = 0 \tag{2.8}$$

$$\Delta E = \frac{1}{2}M\left(v_f{}^2 - v_i^2\right) + \frac{1}{2}I\left(\omega_f^2 - \omega_i^2\right) = 0 \tag{2.9}$$

where ΔP is the change of body momentum, v_i and v_f are the body velocity before and after the collision, ΔL_{beam} is the change of angular momentum of the beam, F is the interaction force acting on the body from the beam, ω_i and ω_f are the angular

velocity before and after the collision, r is the distance from the joint to contacting point, ΔL_{sys} is the change of angular momentum in the system, and ΔE is the change of energy in the system.

2.2.3   Limitation of collision method

The convergence of continual collisions requires objects to have opposite moving trends and depart away after each collision. In the discrete simulation, collisions should not happen in two adjacent time steps, because extra time steps between two collisions are need to update the integration and depart the objects. During continual collisions, kinetic energy is dissipated by a series of collisions because of inelasticity and numerical error. The collision size is decreasing and eventually smaller than the time step size. This phenomenon is called the Zeno behavior that infinite collisions happen in a finite time [27]. It will lead to a significant increase in numerical error.

This problem only arises when the relative normal velocity is at a low level. One solution to this problem is to assume that there is no normal relative movement, and the objects are closely attached. However, the collision method is not suitable under this assumption and I have to find an alternative approach in this situation.

2.3 Constraint method

The constraint method solves the whole system by Newton's second law (Eqn. 2.1, 2.2) and geometric constraints. The motion is constrained by the contact interface. At the contacting points, the body and beam share the same velocity along the normal direction (Eqn. 2.10, 2.12). After taking time derivation of the velocity constraint, the equation with accelerations (Eqn. 2.11, 2.13) can be obtained. The solver is also different with different contact cases.

In the tangent contact case, the velocity constraint is:

$$\omega r = -\sin\theta v_x + \cos\theta v_y \tag{2.10}$$

After time derivation of Eqn. 2.10:

$$\beta r + sin\theta a_x - cos\theta a_y + \left(\frac{x}{r} + cos\theta\right)\omega v_x + \left(\frac{y}{r} + sin\theta\right)\omega v_y = 0 \tag{2.11}$$

where (x, y) is the center of mass measured from the beam joint, $r = \sqrt{x^2 + y^2 - R^2}$ is the distance from the joint to the contact point, R is the radius of the body, θ is the rotated beam angle, ω is the beam angular velocity, β is the beam angular acceleration, (v_x, v_y) is the body velocity, and (a_x, a_y) is the body acceleration.

17

In the point contact case, the velocity constraint is:

$$\omega L \left(\sin\theta x - \cos\theta y\right) = \left(L\cos\theta - x\right) v_x + \left(L\sin\theta - y\right) v_y \qquad (2.12)$$

After time derivation of Eqn. 2.12:

$$\beta L \left(\sin\theta x - \cos\theta y\right) = \left(L\cos\theta - x\right) a_x + \left(L\sin\theta - y\right) a_y - v_x{}^2 - v_y{}^2$$
$$+2L\omega \left(\cos\theta v_y - \sin\theta v_x\right) - L\left(\cos\theta x + \sin\theta y\right)\omega^2 \qquad (2.13)$$

where L is the length of the beam.

By simultaneous equations 2.1, 2.2 and either 2.12 or 2.13, a constraint solver can be setup to solve the accelerations of body and beam, along with the interaction forces F_{resis}. If the solver gives a negative solution to the interaction force, it means the detachment should happen at this step. Then the solver will be called again with the corresponding interaction force assigned to 0.

2.4 Integration of methods and workflow

The constraint method requires two prerequisites: (1) The body and beam have contact. (2) No relative normal velocity at the contacting interface. So, it cannot independently simulate the whole process because the objects need to collide at the

initial contact. The collision method also has the Zeno behavior issue during low

relative normal velocity. So, two methods are integrated as the workflow shown in

Fig. 2.5.
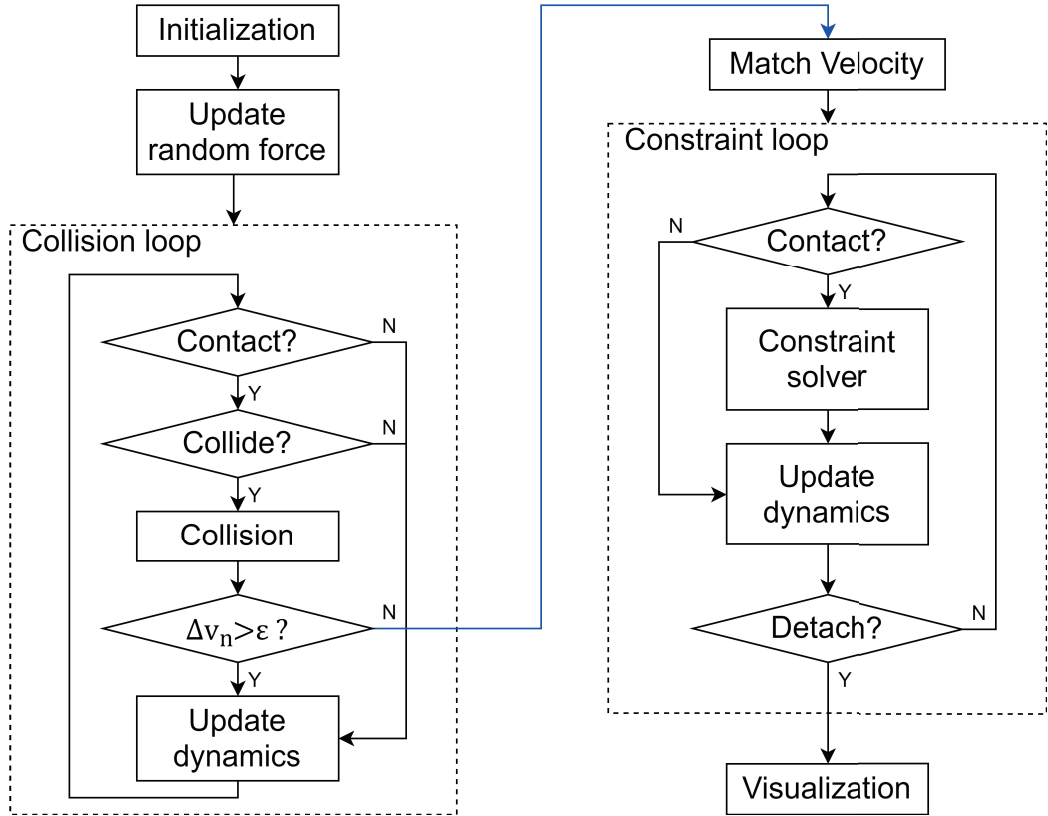
Figure 2.5: A flowchart of the simulation program.

The program will first enter the collision method loop when the body makes initial

contact with the beams. As collisions continue, the relative normal velocity Δv_n of

each collision will be dissipated. When it is lower than a threshold ε, it will stop the

collision method loop and enter the constraint method loop. During the transition,

the beam angular velocity will be updated according to the body velocity to meet the

velocity constraint (Eqn. 2.10, 2.12). In the constraint method loop, the detachment

is determined by the solution of interaction force. If both beams are detached, the program will start again from the collision method loop and waiting for a new initial collision. After the dynamics part is finished, the result will be visualized in a video.

2.5 Potential energy landscape

The potential energy landscape is a modeling approach that helps understand how self-propelled animals' and robots' probabilistic locomotor transitions in complex terrain emerge from physical interaction. In this model, the potential energy comes from the elastic beam joints. In order to traverse, the body needs to push forward and deflect the beams, increasing the elastic potential energy, which results in potential energy barriers on the landscape (Fig. 2.6 (a)(d)). Each beam can form a single barrier, a part of the section area with a radius equals to $L + R$ (Fig. 2.6 (c)). And two barriers overlap in the middle area where the body can interact with both beams.
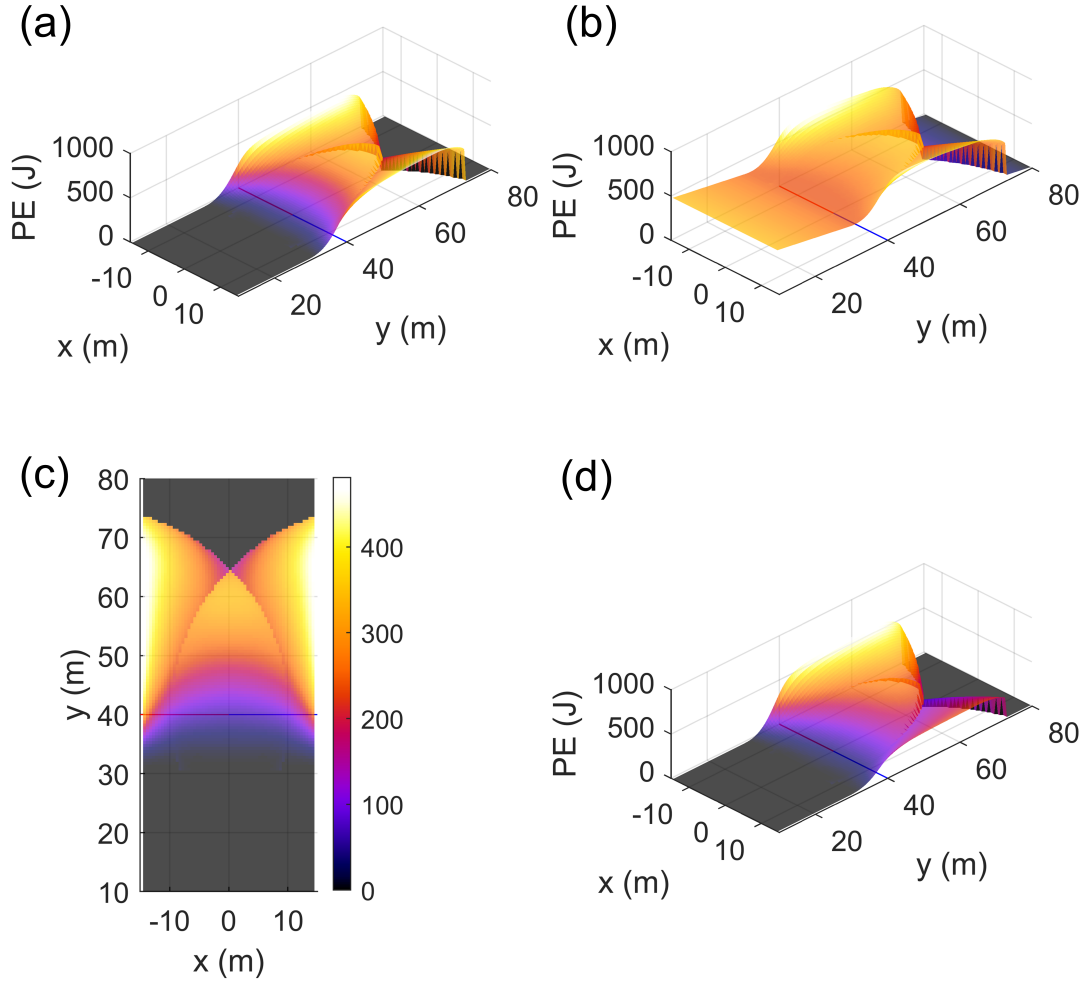
Figure 2.6: Potential energy landscape for the beam obstacle traversal. (a) Landscape with only the elastic energy. The stiffness of each beam is 400 Nm/rad. (b) Landscape with both elastic energy and propulsive conservative energy. The stiffness of each beam is 400 Nm/rad. (c) A top view of the landscape. (d) An asymmetric landscape with left stiffness = 500 Nm/rad and right stiffness = 250 Nm/rad.

The potential energy landscape is calculated (Eqn. 2.14) with the assumption that the beams are always attached to the body in the contact-possible region (middle overlapped area) and deflected forward. The trajectory with actual potential energy from the dynamic simulation can be plotted over the landscape surface.

$$E_{beam} = \frac{1}{2}k_1\theta_1^2 + \frac{1}{2}k_2\theta_2^2 \qquad (2.14)$$

where E_{beam} is the potential energy of the beams, k_i is the elastic stiffness of the ith beam, $i = 1, 2$ for the left and right beam respectively, and θ_i is the rotated angle of the ith beam.

Typically, the actual potential energy is slightly higher than the statically computed value due to the collisions. However, in certain cases, the body can locate in the overlapped area but only interact with a single beam (Fig 2.7 (a)). On the landscape, the trajectory penetrates the landscape surface (Fig 2.7 (b)) and actually moves along the single right energy barrier (Fig 2.7 (c)).
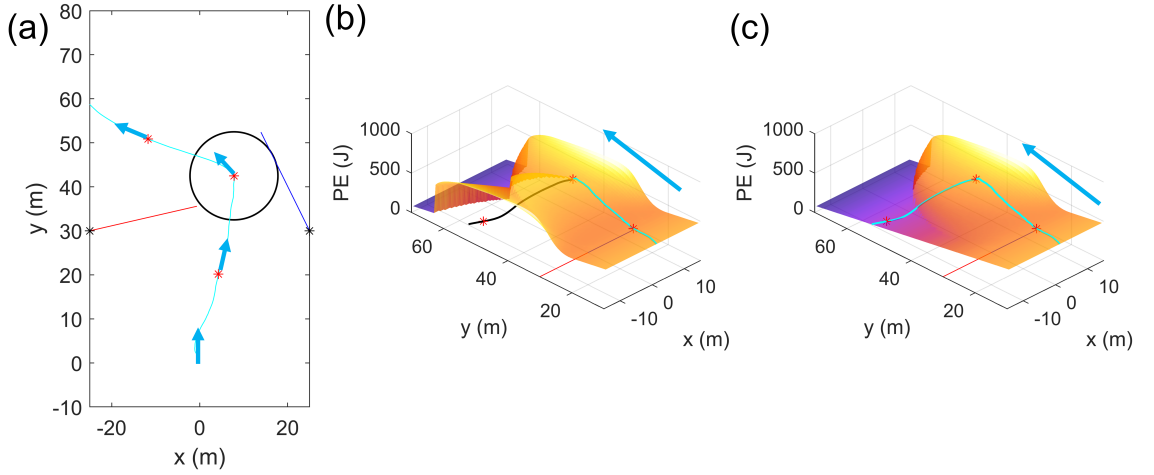
Figure 2.7: An example of trajectory penetrating the landscape surface. Points with $*$ show the mapping between 2D position and landscape. (a) The body interacted with both beams initially, but the left beam first detached while the body was still in the middle overlapped region. (b) The trajectory on the whole landscape. It penetrated the surface when the left beam detached. The cyan curve is the part of trajectory before penetration and the black curve is after penetration. (c) The trajectory on the single right landscape without the inactive barrier. The trajectory can be better visualized after the penetration.

The potential energy landscape can also take the conservative energy of the self-propulsive force into consideration (Fig. 2.6(b)). Because the propulsive force is constant in its direction and magnitude, it is a conservative force. So, it can be assumed that there is a potential energy (Eqn. 2.15) from the propulsive force. The zero level of propulsive energy is defined at the ending boundary where $y_0 = 60$ m. The energy landscape is the sum of elastic energy from beams and propulsive energy from the self-propulsive force (Eqn. 2.16). The random force will add mechanical energy, while the collision and damping will dissipate mechanical energy.

$$E_{prop} = F_{prop} \left(y_0 - y \right) \tag{2.15}$$

where E_{prop} is the propulsive potential energy, and y is the y-direction displacement

of the body measured from the initial position.

The total potential energy is:

$$E_{total} = E_{prop} + E_{beam} = F_{prop} \left(y_0 - y \right) + \frac{1}{2} k_1 \theta_1^2 + \frac{1}{2} k_2 \theta_2^2 \tag{2.16}$$

where E_{total} is the sum of potential energy used in the landscape as Fig. 2.6.

2.6   Extension on multi-obstacle field

Based on the realization of one pair of beam obstacles, I studied an extension to a

larger field with multiple obstacles as a complex terrain. I created a gate lattice that

allows the body to traverse a lattice of "gate-like" obstacles. Fig. 2.8 shows a 9-by-9

gate lattice terrain.
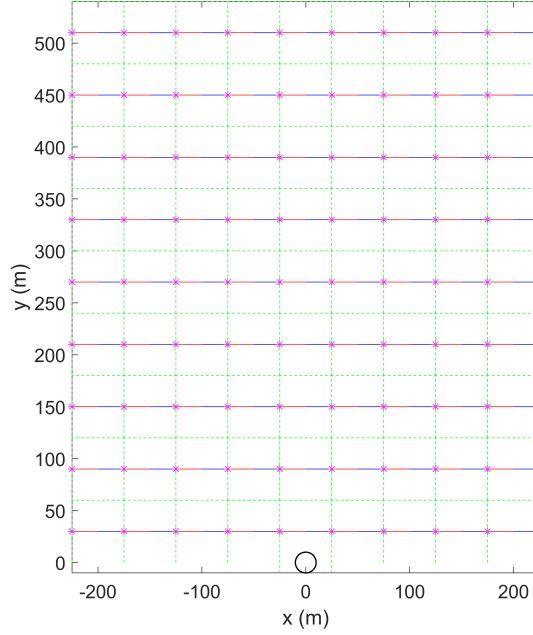
Figure 2.8: A 9-by-9 gate lattice field. i_x ranges from - 4 to 4. i_y ranges from 0 to 8. Each gate region is divided by the green dash lines. The $*$ mark the position of joints. The blue/red lines represent the left/right beam.

The simulation of the gate lattice is based on the reuse of single gate simulation. Each gate is considered individually with the starting position from the exiting position of the last neighbor gate region. The exiting position will be the next starting position when the body transits to the next gate region. An index variable $i = [i_x, i_y]$ is used to track the current active gate. i_x tracks the vertical gates, and i_y tracks the horizontal gates. The output of the main program will be the raw $[x, y]$, where $x \in [-25, 25]$, $y \in [0, 60]$, which is locally restricted within a single gate region. Later in the visualization process, by using the index i, the raw data $[x, y]$ can be converted into the actual position $[X, Y]$, where $X \in [-225, 225]$, $Y \in [0, 540]$, in the whole

region (Eqn. 2.17) .

$$
\begin{cases}
X = x + 50 * i_x, \\
\\
Y = y + 60 * i_y
\end{cases}
\tag{2.17}
$$

The pseudo code:

Algorithm 1 Gate lattice simulation

Initialization, $i \leftarrow [0, 0]$
while $i_x^{min} \leq i_x \leq i_x^{max}$ **and** $i_y^{min} \leq i_y \leq i_y^{max}$ **do**
    Single gate simulation
    if Reach left boundary, $x = -25$ **then**
        $i_x \leftarrow i_x - 1$
        $x \leftarrow x + 25$
    else if Reach right boundary, $x = 25$ **then**
        $i_x \leftarrow i_x + 1$
        $x \leftarrow x - 25$
    else if Reach top boundary, $y = 60$ **then**
        $i_y \leftarrow i_y + 1$
        $y \leftarrow y - 60$
    end if
end while
return $RawData.mat$

function MAT2AVI($RawData.mat$)
    Convert raw position data, $[X, Y] \leftarrow [x, y]$
    Visualization
    return video.avi
end function

2.7 Robot experimental setup

Besides the simulation model, I also developed a simple robot for future experiments. The prerequisites of this physical model need to be a low-friction 2D surface

and a self-propelled car-like robot. A toy hovercraft is a easily accessible choice for the body. The hovercraft (Fig. 2.9 (b) has a pair of front propellers that provide lift to reduce friction and a pair of rear propellers that provide thrust to move forward. The randomness was provided by an electromagnetic oscillator vibrating laterally. The electromagnetic oscillator was controlled by Arduino through a relay. The experiment was set on the air table (Fig. 2.9 (a)) to further reduce the friction.
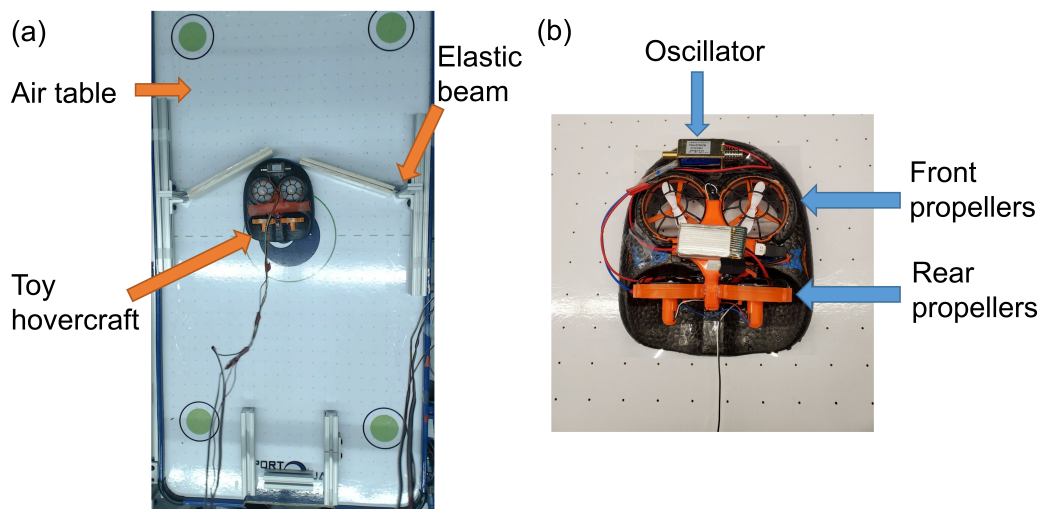
Figure 2.9: The real experimental robot setup. (a) The hovercraft moves on the air table with beam obstacles. (b) The modified hovercraft with an oscillator providing randomness and rear propellers providing propulsive force. The front propellers provide lift to reduce friction.

This real robot is still simple and has several differences from the simulation. 1) the real robot doesn't have a perfectly circle shape, and mass is not equally distributed. 2) the hovercraft has a simple circuit and not suitable for precise control. 3) the real robot will change orientation due to external torque. The propulsive force is constant along the body orientation. 4) the electromagnetic oscillator vibrates by the repeated

collision of a mass inside. It is different from the Gaussian random force used in the simulation. 5) the impact of friction cannot be neglected. These differences give us some insights about what need to be considered in further simulation work to better emulate the real physics.

Chapter 3

Simulation Results

3.1 Probability of traversal

3.1.1 Test configuration

The first result in my model is whether the body traverses successfully or becomes stuck by the beams. A probability of traversal can be obtained by a large number of simulation trials. The run-time of each trial varied from 5 to 20 min on the lab workstation. In this test, uniform beam obstacles are used so that the energy barriers on the landscape is symmetric and the measurement in the test is the displacement in the y-direction. The stiffness of each beam is set to 400 Nm/rad.

Intuitively, the self-propulsive force is the major factor that affects the traversal. Based on our understanding of the landscape, the energy barriers serve as an exchange

between kinetic energy and potential energy. For a higher self-propulsive force, and the system can accumulate more kinetic energy during the acceleration stage before interacting with beams. Traversal will fail when there is no sufficient kinetic energy in the system.

Random force is another factor to increase kinetic energy in the system when it does positive work to the body. It can be expected that the energy fluctuation will be higher than the case without any randomness.

The first hypothesis H1 is formulated.

Hypothesis 1 (H1). *The body has a higher probability of traversal over symmetric beam obstacles under larger self-propulsive force and random force.*

To test H1, I varied the self-propulsive force from 4 N to 9 N with an increment of 1 N and the random force magnitude from 0 N 10 to 40 N with an increment of 10 N. The test configuration is shown in Table 3.1. In each group, there were 100 trials.

Table 3.1: Symmetric test configuration

Parameter	Value
Propulsive force F_{prop}	4,5,6,7,8,9 N
Random force magnitude Rm	0,10,20,30,40 N
Beam stiffness k_1, k_2	400 Nm/rad
Beam damping d_1, d_2	50 Ns/rad
Initial velocity v_0	0 m/s
Coefficient of Restitution CoR	0.8
Oscillator frequency f	50 Hz
Acceleration distance	20 m
Max iterations	3000
Trials per group	100

3.1.2 Result of traversal probability

The criterion of traversing successfully is that the body can reach $y = 65$ m, where the body is out the workspace of beams. Failure resulted from: (1) body gets stuck by the beams, (2) body deviates from the desired track and exits from the side boundaries ($x \leq$ - 25 m or $x \geq 25$ m), and (3) body did not reach $y = 65$ m within max iterations or time limitation.

Fig. 3.1 shows the traverse probability of each group.
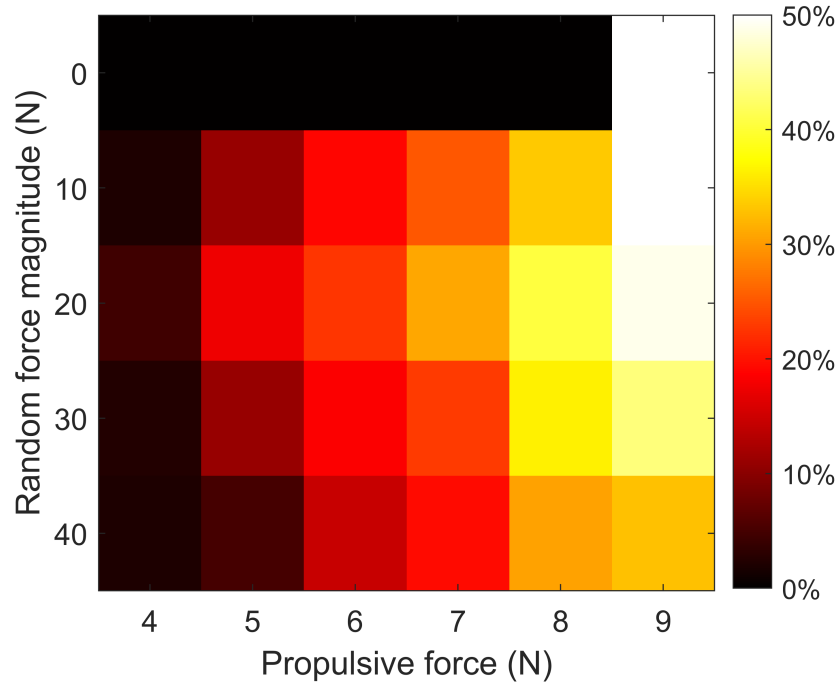
Figure 3.1: The probability table of the symmetric test. The x-axis is the increasing propulsive force, and the y-axis is the random force magnitude.

The propulsive force part of H1 is supported by Fig. 3.1. The propulsive force dominates in the traversal in the range of parameter space tested. An increasing

propulsive force increases the probability of traversing on symmetric beam obstacles, which is in line with H1.

H1 about random force is not completely correct. The random force, when its magnitude increases from 0 N to 20 N, can also help in increase the traversal probability. However, if the random force magnitude further increases from 20 N to 40 N, the probability will decrease. The reason is that under high lateral random force, the body is more likely to have a large lateral velocity, leading to a large displacement and ultimately exiting from the side boundaries. The side-exiting effect is more evident when the $F_{prop} = 9$ N, at which the body is expected to traverse at 100% probability.

Overall, It can be concluded that sufficient but not excessive lateral random force can help traverse symmetric beam obstacles.

3.2 Effect of asymmetry

3.2.1 Test configuration

In the natural environment, the obstacles are rarely symmetric distributed. We are curious about how the body will interact with asymmetric beam obstacles in stiffness. In this test, the right beam stiffness was set to be constant ($k_2 = 500$ Nm/rad) while the left beam stiffness k_1 was varied from 100 Nm/rad to 500 Nm/rad with an increment of 50 Nm/rad. Because the potential energy barrier height is proportional to beam stiffness, it can be expected for a lower left barrier than the

right one. The second hypothesis H2 is formulated.

Hypothesis 2 (H2). *Asymmetry of the potential energy landscape will lead to an increased traversal probability on the lower barrier side.*

To test H2, the self-propulsive force is set from 7 N to 9 N with an increment of 1 N and the random force magnitude is varied from 10 N to 60 N with an increment of 10 N. Here I chose higher random force magnitude than in the symmetric test because I wanted to test whether the randomness will impact the asymmetry. Table 3.2 shows the test configuration.

Table 3.2: Asymmetric test configuration

Parameter	Value
Propulsive force F_{prop}	7,8,9 N
Random force magnitude Rm	10,20,30,40,50,60 N
Left beam stiffness k_1	100:50:500 Nm/rad
Right beam stiffness k_2	500 Nm/rad
Beam damping d_1, d_2	50 Ns/rad
Initial velocity v_0	0 m/s
Coefficient of Restitution CoR	0.8
Oscillator frequency f	50 Hz
Acceleration distance	20 m
Max iterations	3000
Trials per group	100

3.2.2   Result of asymmetric tests

In order to distinguish the different traversals over either the left energy barrier or the right one, I need to classify the trajectory into the left or right type. The criterion is the direction of lateral velocity at the ending boundary ($y = 80$ m). If the body

crosses the left energy barrier, it will have more interaction with the left beam and be deflected to the right, and finally having a positive velocity at x-direction. Similarly, the right type will have a negative velocity at x-direction when it reaches the ending boundary.

The number of left type trials versus right type trials changes in response to the level of asymmetry. Fig. 3.2 shows the trajectory distribution of three selected groups ($F_{prop} = 8$ N and $Rm = 30$ N). The traversal types are distinguished by different colors while the failure trials are gray lines. In the symmetric control group (Fig. 3.2(a)), the trajectories are also roughly symmetric about the y-axis. The probabilities of left and right traversal are similar (22%, 19%). As the left beam stiffness reduced (Fig. 3.2(b)), the probability of left traversal largely increased (46%) while the right one was almost unchanged (18%). When the left beam stiffness further reduced (Fig. 3.2(c)), the traversal of both left and right type become easier (40%, 46%). Those probability changes support the H2.
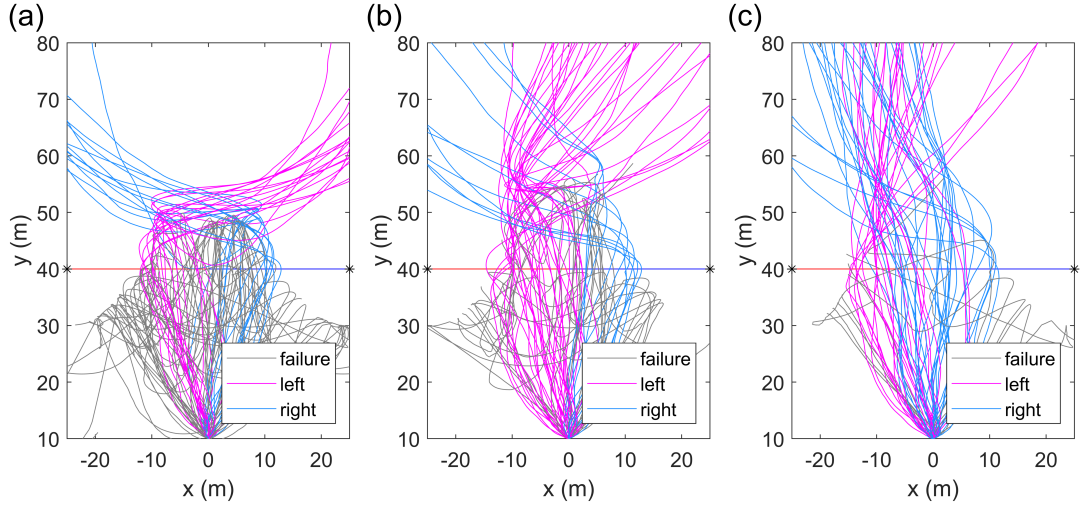
Figure 3.2: Trajectory distribution in asymmetric test. (a) stiffness ratio $=$ $500 : 500$. (b) stiffness ratio $= 300 : 500$. (c) stiffness ratio $= 100 : 500$. self-propulsive force $= 8$ N, random force magnitude $= 30$ N for all groups.

The verification of H2 can be better explained by the energy barriers. Fig. 3.3 shows another three selected group of trajectories plotted over the landscape ($F_{prop} =$ 7 N and $Rm = 10$ N). It gives us a more direct view of the energy barriers traversal. In the symmetric control group (Fig. 3.3(a)), the energy barriers are higher compared with self-propulsive force. Only a few trials can pass by "penetration" (13%, 18%). In Fig. 3.3(b), the left energy barrier is reduced and more trials initially contact with the left beam could traverse (52%) while the right ones remain blocked (0%). In Fig. 3.3(c), the left beam stiffness is much lower than the right beam and the total traversal probability becomes 100%. Here the right energy dominates and deflects most trial to the left. More trails are classified into right types (86%). The left energy barrier is too weak and only deflects only 12% trials. Though most trials are classified into right type, the trajectories flow over the left barrier (Fig. 3.3(c)).
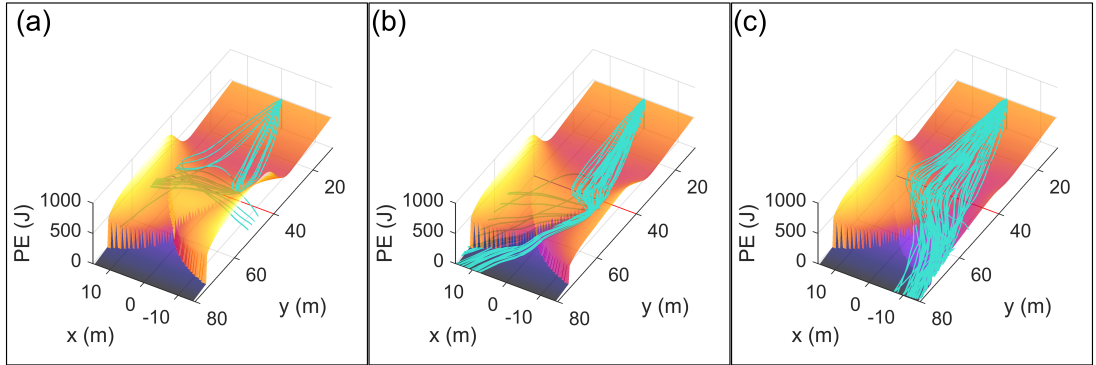
Figure 3.3: Successful trajectories on the landscape in asymmetric test.
Self-propulsive force = 7 N, random force magnitude = 10 N. (a) stiffness ratio = 500
: 500. (b) stiffness ratio = 300 : 500. (c) stiffness ratio = 100 : 500.

From the cases above, the classification of left/right does not match closely with
the traversal over left/right energy barrier. By combining the trajectory distribu-
tion and energy landscape, it can be concluded that the lower barrier side on an
asymmetric landscape have more chance of traversal.

The probability with full-scale of the stiffness ratio (Fig. 3.4(a)) can better show
the exchange between left/right trials. There are different trends divided by the 350
: 500 group. From 500 : 500 to 350 : 500, traversal on the left side becomes more
feasible. From 350 : 500 to 100 : 500 the right barrier becomes dominant over the
left barrier and there are more trials traversing on the right side.

By using a larger range of randomness, the effect of randomness on asymmetry
can also be tested. Fig. 3.4(b) shows when the stiffness ratio is 300 : 500, how the
traversal probability changes with random force magnitude. As Rm increases, the
difference between left and right traversal probability dimnishes. This means that a

high lateral random force can moderate the effect of asymmetry.
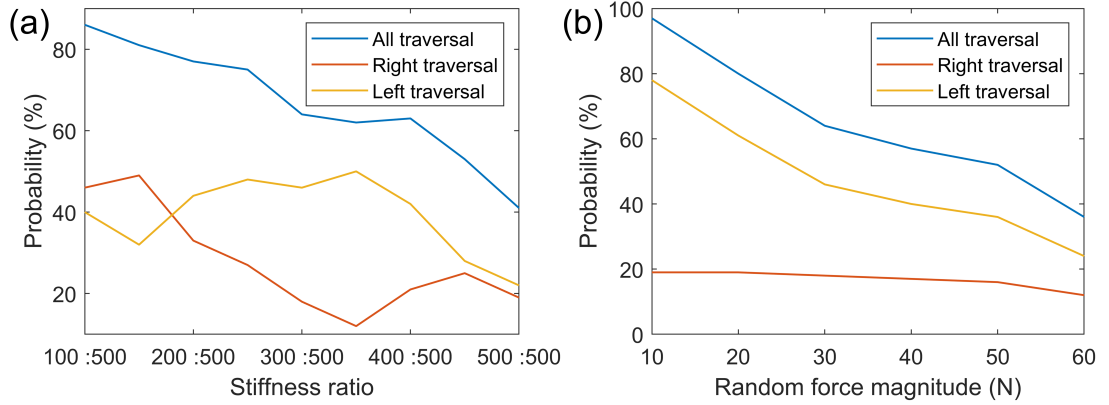
Figure 3.4: Traversal probability in asymmetric test. (a) Propulsive force =
8 N, Random force magnitude = 30 N. (b) Propulsive force = 8 N, Stiffness ratio =
300 : 500.

3.3 Multi-obstacle field simulation

The simulation of a larger field of multiple obstacles focuses on the overall behavior
among the obstacles, just like how animals navigate through complex terrain. Here I
test on the 9 by 9 gate lattice to answer two questions: (1) How will the trajectory
respond to the stiffness distribution in the gate lattice? (2) Is it possible to statistically
predict transition probability to a nearby gate region and eventually predict the whole
behavior.

To test the first question, I designed a C-shape low stiffness track (Fig. 3.5(a)) by
setting the stiffness in gate lattice. Each group has 20 trials with $F_{prop} = 6$ N and
$Rm = 30$ N. 35% trials finally reached the ending boundary ($y = 540$ m). However,

based on the trajectory distribution, there was no pattern as expected that responds to the stiffness "track". The body was more likely to be stuck in the first four rows and it is easier to traverse in the last few rows. At each gate, the kinetic energy and potential energy do not match very well so that the traversal difficult is not uniform along different rows. A potential way to improve this is to tune the parameters, such as increasing damping to the motion and increasing the initial velocity.
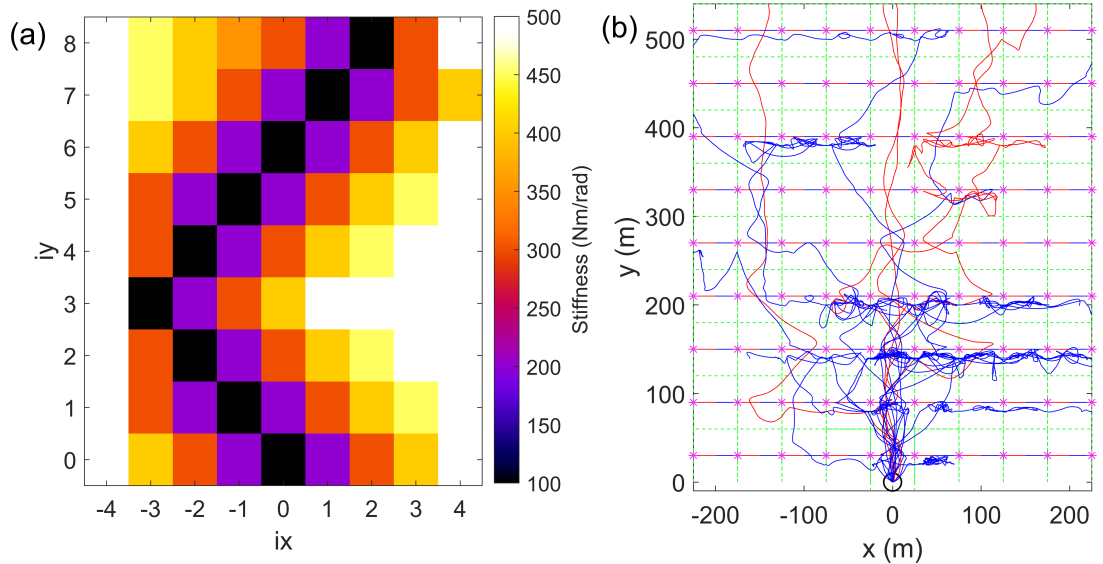
Figure 3.5: Gate lattice with designed track. (a) Stiffness distribution in colormap. (b) Trajectory distribution for 20 trials at $F_{prop} = 6$ N, $Rm = 30$ N. The blue trajectories are the trials reach the ending boundary, while the rest trails are in red lines.

To test the second question, I need to obtain the probability of transitions from one single gate region to the nearby gates (left, right, top, and bottom). By applying the stochastic theory such as the Markov model [28], I can predict a series of transitions over the terrain and compare with the dynamic simulation. Finally, a mathematic

model can be formulated to predict the transitions over the larger-scale terrain. This work is still ongoing. The challenge is that the probability of a single-gate transition varies with to many factors, such as the initial state.

Chapter 4

Conclusion and Discussion

4.1 Conclusion

In this study, a simulation 2D model was setup to predict the beam obstacles traversal and used for testing the hypothesis about the potential energy approach in a fully dynamic situation. It is discovered that the probability of traversal is affected by the input kinetic energy and potential energy barrier. For a self-propelled body, an increasing self-propulsive force can facilitate the traversal. A sufficient but not excessive lateral random force is also helpful in this process. A system with a lateral random force has a higher probability of traversal than a system without randomness. However, an excessive random force does not match with the system and will cause more deviated failure cases. Asymmetry is another critical factor with the obstacle modeled as naturally existed. When the horizontal beams have different stiffness,

asymmetric energy barriers will be formed on the landscape. The body will have more probability to traverse on the lower barrier side. This study also discovered that under high randomness, the difference of probability caused by asymmetry would be moderated. In summary, the potential energy landscape serves as a helpful tool to analyze and understand the beam traversal process.

4.2 Implications for biological and robotics locomotion

This study tested the use the energy-landscape-based approach by studying a stochastic dynamic system. The energy landscape can also be applied in systems that involve conservative forces but difficult to directly measured. Such systems are often observed in animal locomotion, where the interaction is complex (i.e., Terradynamics [29]).

This study reveals the usefulness of the random force, as a form of stochasticity, to overcome resistance. Further in the design of special robots working in extreme environments, we can consider adding extra actuation to provide random perturbing forces to help the robots escape from the trapped state.

The implement of this simulation model also accumulates some experience in the discrete multi-body dynamic simulation. The collision method is suitable to model the stochastic interaction. The constraint method introduces the derivation of the

constraint conditions solved along with equations of motion.

4.3 Limitations and future work

An immediate next step is to continue the work in the multi-obstacle field. The parameters have to be tuned to fit the demands. And massive data is needed to train the Markov model.

One problem with the single gate model is that conclusions of the traversal process are only qualitative. Though I have the statistical results in cases with given parameters and initial states, it is far from predicting the traversal with arbitrary inputs. One potential solution is to train a statistical learning model by the simulation data.

This model is developed for a simplified ideal model system. It needs more complexity to better describe the real system, such as friction, body orientation, body shape, etc. The selected parameters is to test the specific hypothesis but does not match those of a particular biological or robotic system. For example, in the LLS model of the cockroach, the lateral randomness has some match with the self-propulsion force, while such match does not exist in my model in order to test the effect of randomness. However, my simulation setup will provide a stochastic dynamic system model for further studies.

Bibliography

[1] R. M. Alexander, *Principles of animal locomotion.* Princeton University Press, 2003.

[2] G. N. DeSouza and A. C. Kak, "Vision for mobile robot navigation: A survey," *IEEE Transactions on Pattern Analysis and Machine Intelligence*, vol. 24, no. 2, pp. 237–267, 2002.

[3] J. Borenstein, Y. Koren *et al.*, "The vector field histogram-fast obstacle avoidance for mobile robots," *IEEE Transactions on Robotics and Automation*, vol. 7, no. 3, pp. 278–288, 1991.

[4] O. Khatib, *Real-Time Obstacle Avoidance for Manipulators and Mobile Robots.* New York, NY: Springer New York, 1990, pp. 396–404. [Online]. Available: https://doi.org/10.1007/978-1-4613-8997-2_29

[5] C. Li, A. O. Pullin, D. W. Haldane, H. K. Lam, R. S. Fearing, and R. J. Full, "Terradynamically streamlined shapes in animals and robots enhance traversability

through densely cluttered terrain," *Bioinspiration & Biomimetics*, vol. 10, no. 4, p. 046003, 2015.

[6] Q. Xuan and C. Li, "Coordinated appendages accumulate more energy to self-right on the ground," *IEEE Robotics and Automation Letters*, vol. 5, no. 4, pp. 6137–6144, 2020.

[7] C. Harley, B. English, and R. Ritzmann, "Characterization of obstacle negotiation behaviors in the cockroach, *Blaberus discoidalis*," *Journal of Experimental Biology*, vol. 212, no. 10, pp. 1463–1476, 2009.

[8] K. Low, T. Hu, S. Mohammed, J. Tangorra, and M. Kovac, "Perspectives on biologically inspired hybrid and multi-modal locomotion," *Bioinspiration and Biomimetics*, vol. 10, no. 2, 2015.

[9] J. T. Watson, R. E. Ritzmann, S. N. Zill, and A. J. Pollack, "Control of obstacle climbing in the cockroach, *Blaberus discoidalis*. I. Kinematics," *Journal of Comparative Physiology A*, vol. 188, no. 1, pp. 39–53, 2002.

[10] R. Othayoth, G. Thoms, and C. Li, "An energy landscape approach to locomotor transitions in complex 3d terrain," *Proceedings of the National Academy of Sciences*, vol. 117, no. 26, pp. 14 987–14 995, 2020.

[11] J. N. Onuchic and P. G. Wolynes, "Theory of protein folding," *Current Opinion in Structural Biology*, vol. 14, no. 1, pp. 70–75, 2004.

[12] P. Bovet and S. Benhamou, "Spatial analysis of animals' movements using a correlated random walk model," *Journal of Theoretical Biology*, vol. 131, no. 4, pp. 419–433, 1988.

[13] A. A. Faisal, L. P. Selen, and D. M. Wolpert, "Noise in the nervous system," *Nature Reviews Neuroscience*, vol. 9, no. 4, pp. 292–303, 2008.

[14] O. Bénichou, M. Coppey, M. Moreau, P. Suet, and R. Voituriez, "A stochastic theory for the intermittent behaviour of foraging animals," *Physica A: Statistical Mechanics and its Applications*, vol. 356, no. 1, pp. 151–156, 2005.

[15] C. M. Bergman, J. A. Schaefer, and S. Luttich, "Caribou movement as a correlated random walk," *Oecologia*, vol. 123, no. 3, pp. 364–374, 2000.

[16] T. Y. Moore, K. L. Cooper, A. A. Biewener, and R. Vasudevan, "Unpredictability of escape trajectory explains predator evasion ability and microhabitat preference of desert rodents," *Nature Communications*, vol. 8, no. 1, pp. 1–9, 2017.

[17] M. D. McDonnell and L. M. Ward, "The benefits of noise in neural systems: bridging theory and experiment," *Nature Reviews Neuroscience*, vol. 12, no. 7, pp. 415–425, 2011.

[18] Q. Xuan and C. Li, "Randomness in appendage coordination facilitates strenuous ground self-righting," *Bioinspiration & Biomimetics*, vol. 15, no. 6, p. 065004, 2020.

BIBLIOGRAPHY

[19] C. Li, T. Wöhrl, H. K. Lam, and R. J. Full, "Cockroaches use diverse strategies to self-right on the ground," *Journal of Experimental Biology*, vol. 222, no. 15, 2019.

[20] L. Frantsevich, "Righting kinematics in beetles (insecta: Coleoptera)," *Arthropod Structure & Development*, vol. 33, no. 3, pp. 221–235, 2004.

[21] G. Panganiban, S. M. Irvine, C. Lowe, H. Roehl, L. S. Corley, B. Sherbon, J. K. Grenier, J. F. Fallon, J. Kimble, M. Walker *et al.*, "The origin and evolution of animal appendages," *Proceedings of the National Academy of Sciences*, vol. 94, no. 10, pp. 5162–5166, 1997.

[22] G. Li, W. Li, J. Zhang, and H. Zhang, "Analysis and design of asymmetric oscillation for caterpillar-like locomotion," *Journal of Bionic Engineering*, vol. 12, no. 2, pp. 190–203, 2015.

[23] B. P. Selgrade, M. Thajchayapong, G. E. Lee, M. E. Toney, and Y.-H. Chang, "Changes in mechanical work during neural adaptation to asymmetric locomotion," *Journal of Experimental Biology*, vol. 220, no. 16, pp. 2993–3000, 2017.

[24] J. Schmitt and P. Holmes, "Mechanical models for insect locomotion: dynamics and stability in the horizontal plane I. Theory," *Biological Cybernetics*, vol. 83, no. 6, pp. 501–515, 2000.

BIBLIOGRAPHY

[25] P. M. Hubbard, "Interactive collision detection," in *Proceedings of 1993 IEEE Research Properties in Virtual Reality Symposium*. IEEE, 1993, pp. 24–31.

[26] M. Moore and J. Wilhelms, "Collision detection and response for computer animation," in *Proceedings of the 15th Annual Conference on Computer Graphics and Interactive Techniques*, 1988, pp. 289–298.

[27] A. D. Ames, A. Abate, and S. Sastry, "Sufficient conditions for the existence of Zeno behavior," in *Proceedings of the 44th IEEE Conference on Decision and Control*. IEEE, 2005, pp. 696–701.

[28] R. S. Sutton and A. G. Barto, *Reinforcement learning: An introduction*. MIT press, 2018.

[29] C. Li, T. Zhang, and D. I. Goldman, "A terradynamics of legged locomotion on granular media," *Science*, vol. 339, no. 6126, pp. 1408–1412, 2013.